LNEG
Laboratório Nacional de Energia e Geologia, I. P.

HR EXCELLENCE IN RESEARCH

NewSOL Project (720985)

Thermal calculations for TES tank predesign: EMSP case-study

Pedro Azevedo

May, 2017

Estrada do Paço do Lumiar, 22
1649-038 LISBOA - Portugal
Tel: +351 210 924 600/1
Fax: +351 217 166 966 Online: 217166966@fax.ptprime.pt
www.lneg.pt

REPÚBLICA PORTUGUESA
ECONOMIA

Copyright notice

LEN-UER-2017-N02-IR
"Thermal calculations for TES tank predesign: EMSP case-study"
Internal Report on work developed by LNEG included in Task 2.2 "Predesign of tank and module system architectures" for partial fulfillment of deliverable D2.1 "Preliminary selection of materials compositions and TES system predesign".
Azevedo, Pedro
May, 2017

Table of contents

List of figures

List of tables

Overview

LNEG is one of the partners involved in Task 2.2 "Predesign of tank and module system architectures". The present document reports work developed by LNEG for partial fulfillment of deliverable D2.1 "Preliminary selection of materials compositions and TES system predesign". Preliminary data were already published in Azevedo (2017) and on D2.1 "Preliminary selection of materials compositions and TES system predesign".

The present document presents the efficiency approach and the methodology for heat losses and temperature inside the walls calculations. Additionally, the EMSP is hereby described as a case-study and its dimensions, materials, and the aforementioned heat losses and temperature inside the walls, were estimated.

Most of the results already published or hereby updated will be "the starting point to set the thermal and mechanical conditions for detailed modelling in WP5 and demonstration of the NewSOL concept in WP6", as described in Task 2.2. The "definition of a reasonable number of its layers", also stated in the same Task, was not addressed in this document, although some remarks are presented in the last section of this document.

In the same way, the definition of maximum and minimum mass flows in the solar field were not clearly defined. Based on the peak power of the solar field, a maximum mass flow was considered for charging the TES tank and the same mass flow was considered for the discharge stage. The minimum mass flow was not defined in this document as discussed in section "Molten salts mass flow".

This document is complementary to Azevedo (2017). Some design values published in that document were updated in D2.1 or hereby, namely the minimum temperature of the molten salts, and some additional considerations were implemented in the calculations, such as two different materials in the foundation of the tank and a specific constraint of temperature in the structural concrete layer. This constraint evolved to the calculation of the temperature in each layer of the TES boundaries.

Finally, the "concluding remarks" present the rationale for open questions with regard to the tank dimensions, namely the turbine data, the buffer height, as well as to reopen the materials/dimensions question with regard to the temperature inside the walls constraint. Additionally, some comments are made addressing the solid/liquid layers to include inside the tank.

Methodology

The new methodology includes two particular conditions. The calculation of heat losses in through the boundaries now includes two different zones in the foundation and the associated heat losses were recalculated layer by layer in order to find the temperatures between layers. The next two sections describe those calculations.

Heat losses

According to Figure 1, the foundation of the tank has now two different zones: an inner zone of lightweight concrete (LWC) and an outer zone of structural concrete (SC). Thus, the heat flux depends on the overall heat transfer coefficient in each of those zones, although the temperature difference between the molten salts and the soil remains the same.

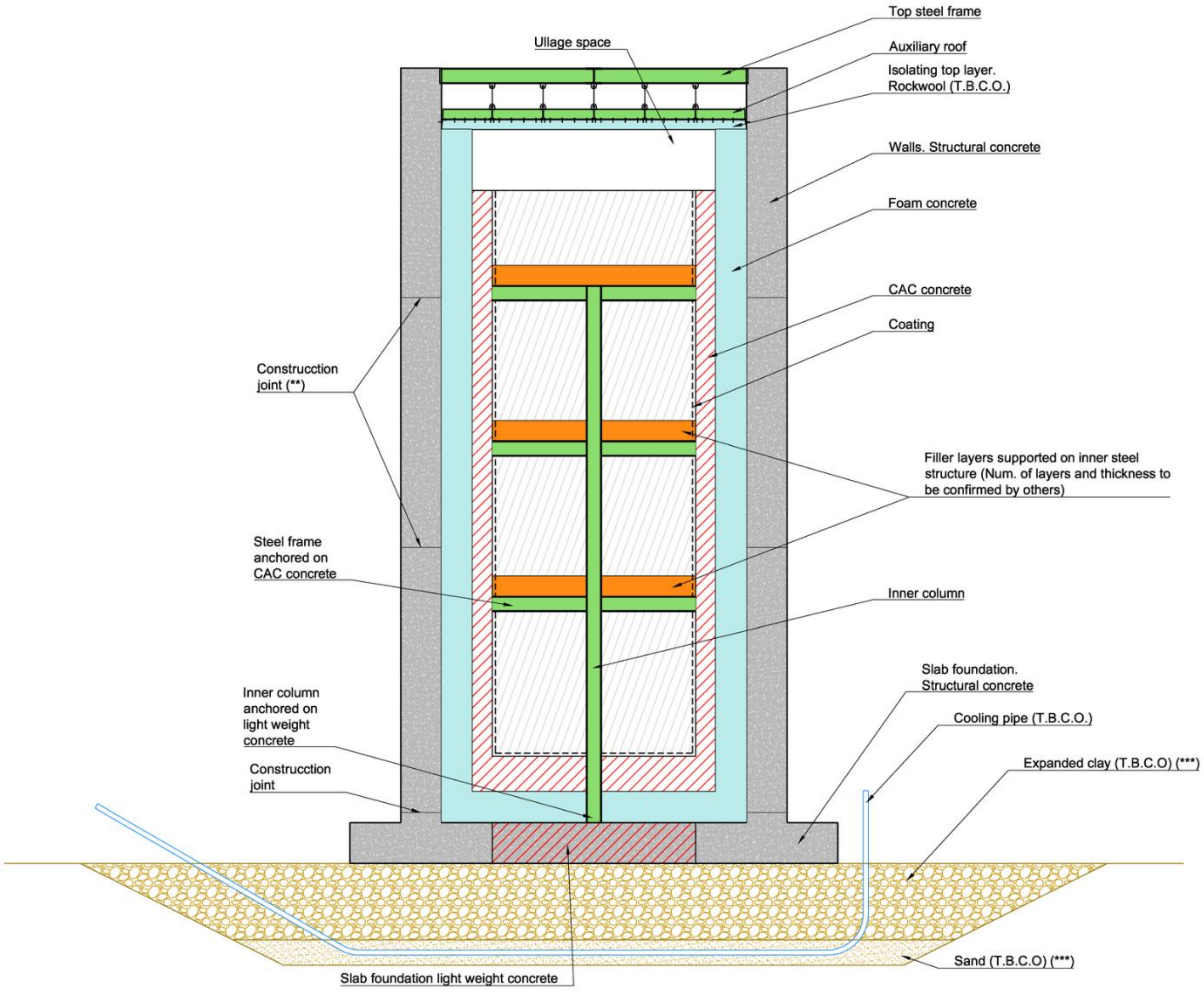

Figure 1: Tank predesign.

Figure 2 describes the heat fluxes flowing through the walls of the tank, as well as the heat flow in the ullage space. The calculations for heat fluxes through the walls are presented in equations (1) to (24) and they account for two different zones in the foundation of the TES tank.

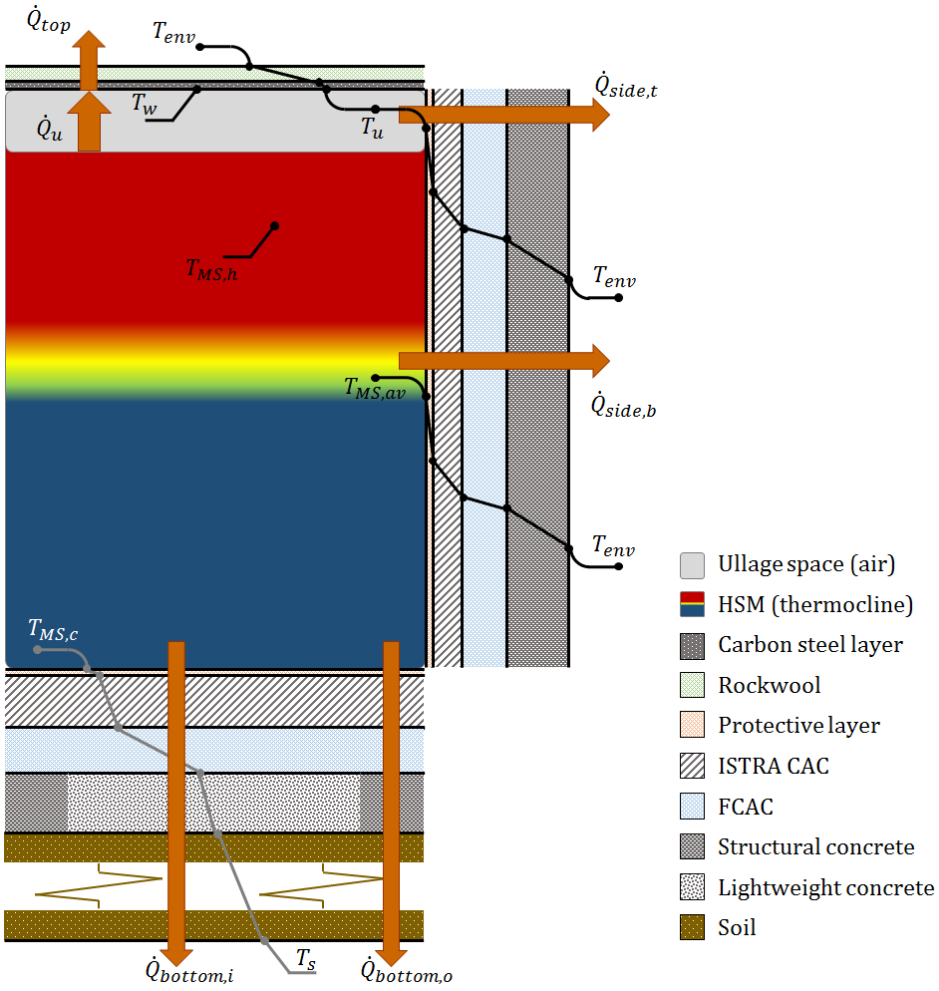

Figure 2: Heat fluxes through the walls and balance to the ullage space.

$$\dot{Q}_{losses} = \dot{Q}_{top} + \dot{Q}_{side\_t} + \dot{Q}_{side\_b} + \dot{Q}_{bottom\_o} + \dot{Q}_{bottom\_i} \quad (1)$$

$$\dot{Q}_{top} = A_{top}.U_{top}.\Delta T_{top} \quad (2)$$

$$A_{top} = \pi.R^2 \quad (3)$$

$$U_{top} = \left(\frac{1}{h_u} + \frac{L_{i,1}}{k_{i,1}} + \frac{L_{i,2}}{k_{i,2}} + \frac{1}{h_{air}}\right)^{-1} \quad (4)$$

$$\Delta T_{top} = T_u - T_{env} \quad (5)$$

$$T_u = \frac{T_{MS,h} + T_w}{2} \quad (6)$$

$$\dot{Q}_{side\_t} = A_{side\_t}.U_{side\_t}.\Delta T_{side\_t} \quad (7)$$

$$A_{side\_t} = 2.\pi.R.L_u \quad (8)$$

$$U_{side\_t} = \left(\frac{1}{h_u} + \frac{L_{i,1}}{k_{i,1}} + \frac{L_{i,2}}{k_{i,2}} + \frac{L_{i,3}}{k_{i,3}} + \frac{L_{i,4}}{k_{i,4}} + \frac{L_{i,5}}{k_{i,5}} + \frac{1}{h_{air}}\right)^{-1} \quad (9)$$

$$\Delta T_{side\_t} = T_u - T_{env} \quad (10)$$

$$\dot{Q}_{side\_b} = A_{side\_b}.U_{side\_b}.\Delta T_{side\_b} \quad (11)$$

$$A_{side\_b} = 2.\pi.R.H_{HSM} \quad (12)$$

$$U_{side\_b} = \left(\frac{1}{h_{MS}} + \frac{L_{i,1}}{k_{i,1}} + \frac{L_{i,2}}{k_{i,2}} + \frac{L_{i,3}}{k_{i,3}} + \frac{L_{i,4}}{k_{i,4}} + \frac{L_{i,5}}{k_{i,5}} + \frac{1}{h_{air}}\right)^{-1} \quad (13)$$

$$\Delta T_{side\_b} = T_{MS,av} - T_{env} \quad (14)$$

$$T_{MS,av} = Ch_{status}.T_{MS,h} + (1 - Ch_{status}).T_{MS,c} \quad (15)$$

$$\dot{Q}_{bottom\_o} = A_{bottom\_o}.U_{bottom\_o}.\Delta T_{bottom\_o} \quad (16)$$

$$A_{bottom\_o} = \pi.R^2 - \pi.(R - L_s)^2 = \pi.\left(2.R.L_s - {L_s}^2\right) \quad (17)$$

$$U_{bottom\_o} = \left(\frac{1}{h_{MS}} + \frac{L_{i,1}}{k_{i,1}} + \frac{L_{i,2}}{k_{i,2}} + \frac{L_{i,3}}{k_{i,3}} + \frac{L_{i,4}}{k_{i,4}} + \frac{L_{i,5}}{k_{i,5}} + \frac{L_{i,s}}{k_{i,s}}\right)^{-1} \quad (18)$$

$$\Delta T_{bottom\_o} = T_{MS,c} - T_s \quad (19)$$

$$\dot{Q}_{bottom\_i} = A_{bottom\_i}.U_{bottom\_i}.\Delta T_{bottom\_i} \quad (20)$$

$$A_{bottom\_i} = \pi.(R - L_s)^2 \quad (21)$$

$$U_{bottom\_i} = \left(\frac{1}{h_{MS}} + \frac{L_{i,1}}{k_{i,1}} + \frac{L_{i,2}}{k_{i,2}} + \frac{L_{i,3}}{k_{i,3}} + \frac{L_{i,4}}{k_{i,4}} + \frac{L_{i,5}}{k_{i,5}} + \frac{L_{i,s}}{k_{i,s}}\right)^{-1} \quad (22)$$

$$\Delta T_{bottom\_i} = T_{MS,c} - T_s \quad (23)$$

Where:

$\dot{Q}_i$: Power losses in boundary *i* [W];

A_i: Surface area in boundary *i* [m²];

U_i: Overall heat transfer coefficients for boundary *i* [W/m²-K];

ΔT_i: Temperature difference between the zones considered for the heat transfer in boundary *i* [K];

$k_{i,j}$: Thermal conductivity for material *i* in layer *j* [W/m-K];

$L_{i,j}$: Length of material *i* in layer *j* [m];

R: Radius of the TES tank [m];

H_{HSM}: Height of the HSM [m];

h_{air}: Convection heat transfer coefficient for air [W/m²-K];

h_u: Convection heat transfer coefficient for ullage space material [W/m²-K];

h_{MS}: Convection heat transfer coefficient for molten malts [W/m²-K];

$T_{MS,h}$: Temperature for "hot" molten salts [K];

$T_{MS,c}$: Temperature for "cold" molten salts [K];

$T_{MS,av}$: Molten salts average temperature [K];

Ch_{status}: Charging status [fraction];

T_{env}: Environment temperature [K];

T_w: Top boundary internal wall temperature [K];

T_u: Ullage space temperature [K];

L_s: Length of structural concrete in foundation [m];

T_s: Soil undisturbed temperature [K];

However, the temperature near the top slab (T_w) is unknown and an additional balance was performed in order to find that temperature, as described in Figure 2. The balance is presented in equations (24) to (28).

$$\dot{Q}_u = \dot{Q}_{top} + \dot{Q}_{side\_t} = A_u.\left[U_u.\Delta T_u + \sigma.\left(\varepsilon_{MS}.T_{MS,h}^4 - \varepsilon_w.T_w^4\right)\right] \quad (24)$$

$$A_u = \pi.R^2 \quad (25)$$

$$U_u = \left(\frac{L_u}{k_u} + \frac{1}{h_u}\right)^{-1} \quad (26)$$

$$\Delta T_u = T_{MS,h} - T_w \quad (27)$$

$$T_w^{(k+1)} = \left\{\frac{1}{\sigma.\varepsilon_w.T_w^{(k)}}.\left[\sigma.\varepsilon_{MS}.T_{MS,h}^4 + U_u.\left(T_{MS,h} - T_w^{(k)}\right) - \left(U_{top}/2 + L_u.U_{side_t}/R\right).\left(T_{MS,h} + T_w^{(k)} - T_{env}/2\right)\right]\right\}^{1/3} \quad (28)$$

Where:

σ: Stefan-Boltzmann constant [5,6704×10^{-8} W/m²-K⁴];

ε_{MS}: Molten Salts emissivity [-];

ε_w: Cover wall (top slab) emissivity [-];

L_u: Height of ullage space [m];

k_u: Thermal conductivity in ullage space [W/m-K];

Temperature in the walls

Once the heat losses through the walls are known, the equations considered for a specific boundary can now be used in order to retrieve the temperature between each layer of that boundary. Considering one of the walls (e.g. the side wall around the ullage space denoted as $side\_t$ and using equations (7) to (10) to calculate the heat losses), the heat flux ($\dot{q}_{side\_t}$) represents the heat losses per unit of area as denoted in equation (29) and that heat flux is constant across all the walls, once a stationary condition is achieved. Thus, knowing the temperature of the fluid inside the tank (T_u) and the particular set of layers to consider (e.g. 4 layers), a partial heat transfer coefficient and temperature difference can be calculated as denoted in equations (30) to (32).

$$\dot{q}_{side\_t} = \dot{Q}_{side\_t}/A_{side\_t} \tag{29}$$

$$\dot{q}_{side\_t} = U_{side\_t\_p}.\Delta T_{side\_t\_p} \tag{30}$$

$$U_{side\_t\_p} = \left(\frac{1}{h_u} + \frac{L_{i,1}}{k_{i,1}} + \frac{L_{i,2}}{k_{i,2}} + \frac{L_{i,3}}{k_{i,3}} + \frac{L_{i,4}}{k_{i,4}}\right)^{-1} \tag{31}$$

$$\Delta T_{side\_t\_p} = T_u - T_{i,5} \tag{32}$$

Case-Study: EMSP

Considering that the minimum temperature of the molten salts changed to 290 ºC, a new calculation of the capacity of the TES tank was also performed. The next sections present the new TES capacity, the heat losses for the efficiency approach and the temperatures between the layers of the walls.

Although, no changes occurred in the molten salts (initially they were defined as solar salt) neither in the filler (remains rock because slag from São Domingos mines were not adequately characterized with regard to porosity and thermal properties), the size of the tank was fixed for the efficiency approach with these materials.

If and when the molten salts or the filler are changed, the autonomous working period for the power block (i.e. the amount of time the power block will operate at nominal power with energy provided by the thermocline tank) can increase or decrease, depending on the new properties.

Thermal energy storage capacity

The complete sizing procedure was already defined in Azevedo (2017). However, some details changed, namely the minimum temperature of molten salts, and the final capacity is hereby presented. However, the solar field, the power block and the autonomous working period remain identical.

The solar field has 1,8 MW_{th}, with the maximum and minimum temperatures[1] of, respectively, 550 ºC and 290 ºC. The solar multiple, as well as the steam conditions for the turbine had to be

[1] Other values can be used depending on the molten salts properties.

estimated and Table 1 presents those operating conditions along with other relevant parameters. To determine the steam conditions for the turbine, a SST-060 Siemens steam turbine was considered, ranging from 0,5 to 6 MW_e. Additional information on the power block is presented in "Concluding remarks" section.

Table 1: Design parameters.

Description	Units	Value
Solar field power output ($\dot{Q}_{solar}$)	[kW_{th}]	1800
Solar multiple (C)	-	1
Efficiency of Rankine cycle and generator (η_R)	[%]	40
Power block output ($\dot{Q}_e$)	[kW_e]	720
Steam temperature @ turbine inlet	[ºC]	530
Steam/water mass flow ($\dot{m}_w$)	[kg/s]	0,663
Autonomous working period	[h]	8
Energy retrieved from storage (Q_{HSM})	[MWh]	16,9

Molten salts mass flow

Table 2 presents the estimated molten salts (MS) thermal conditions and mass flow. Without additional information on the materials, MS were assumed to be Solar Salt (60% $NaNO_3$ – 40% KNO_3) and the mass flow was calculated by equation (35), considering equations (33) and (34).

Table 2: Heat storage material.

Description	Units	Value
Energy retrieved from storage (Q_{HSM})	[MWh]	16,9
Maximum temperature (T_{max})	[ºC]	550
Minimum temperature ($T_{min} = T_{ref}$)	[ºC]	290
MS mass flow ($\dot{m}_{MS}$)	[kg/s]	5,373

$$\dot{Q} = \dot{m}_{MS} \cdot \int_{Tref}^{T} Cp_{MS}\, \partial T \tag{33}$$

$$Cp_{MS}(T) = 1396{,}044 + 0{,}172.T \text{ (R. Serrano-López } et\ al\text{, 2013)} \tag{34}$$

$$\dot{m}_{MS} = \frac{\dot{m}_w . \Delta h_{SG,w}}{h_{in} - h_{out}} \quad (35)$$

Where:

$\dot{Q}$: Molten salts thermal power [kW];

$\dot{m}_{MS}$: Molten salts mass flow [kg/s];

$Cp_{MS}(T)$: Molten salts specific heat [J/kg-K] (with T [K]);

$\Delta h_{SG,w}$: Enthalpy difference in the Steam Generator, on the water side [kJ/kg];

h_{in}: Molten salts enthalpy at SG inlet [kW];

h_{out}: Molten salts enthalpy at SG outlet [kW];

For a different value of DNI or with a different design point of the steam turbine, the MS mass flow rate coming from the collectors can be different from the calculated discharge mass flow rate.

Depending on solar power availability and on operation strategy of the plant, the definition of a minimum mass flow rate implies a discussion around several other parameters, such as:

- Minimum working DNI, defined by the promotor;
- Minimum mass flow considered for the chosen pump by the manufacturer;
- Minimum mass flow considered for the chosen receptor by the manufacturer;
- Analysis of minimum mass flow in the piping in order to endure a certain temperature at the TES tank or at the steam turbine;
- Analysis of minimum energy input in the TES tank with regard to the thermocline degradation occurring over night or in a certain period of time.

Heat storage material

In order to store the calculated amount of energy, it is important to use an adequate reference temperature. In this case, the reference temperature was 290 ºC in order to retrieve the tank "empty" at minimum temperature.

The temperature was considered to vary only in height but to be constant along the radial distance inside the tank. Hence, an effective value for each thermal property was able to be calculated based on the MS property and the filler property and porosity, as denoted in equations (36) and (37). Table 3 presents the main parameters for the TES tank.

$$\phi_{eff} = \varepsilon . \phi_f + (1 - \varepsilon) . \phi_s \quad (36)$$

Where:

ϕ_{eff}: Effective value for property ϕ;

ε: Filler porosity;

ϕ_f: Fluid value for property ϕ;

ϕ_s: Solid value for property ϕ;

$$Cp_{eff}(T) = 1048{,}517 + 0{,}065.T \quad (37)$$

Table 3: Heat storage parameters.

Description	Units	Value
Molten salts: Solar salt		
MS specific heat (Cp_{MS}) @ max temp, R. Serrano-López *et al* (2013)[2]	[kJ/kg-K]	1,538
MS density (ρ_{MS}) @ max temp, R. Serrano-López *et al* (2013)	[kg/m³]	1740
Filler: Rock		
Filler porosity (ε), Anderson *et al* (2015)	[%]	37,5
Filler specific heat (Cp_s), Li *et al* (2011)	[kJ/kg-K]	0,84
Filler density (ρ_s), Li *et al* (2011)	[kg/m³]	2480
Effective material (HSM)		
HSM specific heat ($Cp_{eff,max}$) @ max temp	[kJ/kg-K]	1,135
HSM specific heat ($Cp_{eff,min}$) @ min temp	[kJ/kg-K]	1,116
HSM density ($\rho_{eff,max}$) @ max temp	[kg/m³]	2203
TES data		
HSM mass ($m_{HSM,0}$)	[kg]	214.500
HSM volume ($V_{HSM,0}$)	[m³]	97,4

The buffer height (b) considered for the thermocline was 30% and the period (t) foreseen to feed the turbine in autonomous conditions was 8h. The final values for HSM mass and volume are

[2] Values used for reference purposes only.

presented in Table 4. The ullage space is also defined in Table 4 and, in this case study, the height of the ullage space was defined as 10% of the height considered for the HSM (H_{HSM}).

Table 4: Project data for tank dimensions calculation.

Description	Units	Value
HSM volume (V_{HSM})	[m³]	139,1
MS volume (ε = 37,5%)	[m³]	52,2
Filler volume (ε = 37,5%)	[m³]	87,0
Height of the ullage space (L_u/H_{HSM})	[%]	10

Dimensions

Considering that the Consortium chose the efficiency approach described in Azevedo (2017), only the sizing and dimensions with regard to this approach are addressed in this document.

In this approach, aimed to improve the thermal energy storage (TES) efficiency, equations (37), (40) and (42) define the calculation of the TES efficiency (Flueckiger *et al.*, 2013, Bayón and Rojas, 2014).

$$\eta_{TES} = \frac{Q_{stored}}{Q_{stored,max}} \times 100\% \quad (37)$$

$$Q_{stored} = A_{TES}.H_{hot}.\rho_{eff,max}.Cp_{eff,max}.\Delta T_{max} \quad (38)$$

$$Q_{stored,max} = A_{TES}.H_{HSM}.\rho_{eff,max}.Cp_{eff,max}.\Delta T_{max} \quad (39)$$

$$\eta_{TES} = \frac{H_{hot}}{H_{HSM}} \times 100\% \quad (40)$$

$$H_{hot} = H_{HSM} - (H_{tc} + H_{cold}) \quad (41)$$

$$\eta_{TES} = \left(1 - \frac{H_{tc} + H_c}{H_{HSM}}\right) \times 100\% \quad (42)$$

Where:

η_{TES}: TES efficiency [%];

Q_{stored}: Stored energy considering only the high temperature isothermal zone [kJ];

$Q_{stored,max}$: Stored energy considering all the HSM at high temperature [kJ];

A_{TES}: Area of the base of the tank [m²];

H_{hot}: Height of the high temperature isothermal zone [m];

ΔT_{max}: $T_{max} - T_{ref}$

H_{tc}: Height of the thermocline zone [m];

H_{cold}: Height of the low temperature isothermal zone [m];

Thus, in order to yield the highest efficiency, as denoted by equation (42), the Consortium chose a tank height (H_{TES}) of 12,2 m, including the ullage space, as described by Libby *et al* (2010).

In this approach, several of the discussed variables are calculated according to equations (43) and (44). Table 5 presents the calculated dimensions considering the conditions described above.

$$H_{HSM} = {H_{TES}}/{(1 + x)} \tag{43}$$

$$R = \sqrt{\frac{V_{HSM}}{\pi . H_{HSM}}} \tag{44}$$

Table 5: Dimensions of the tank.

Description	Units	Value
HSM volume (V_{HSM})	[m³]	139,1
TES height (H_{TES})	[m]	12,2
Height of the ullage space (L_u)	[m]	1,11
HSM height (H_{HSM})	[m]	11,09
HSM radius (R)	[m]	1,998

Heat losses and temperature in the walls

According to equations (1) to (28), the calculations for the heat losses considering the tank dimensions are now available. The same occurs for the temperatures inside the walls, as described by equations (29) to (32). Tables 6 to 8 present the data considered in the walls and Table 9 presents the results for heat losses through the walls considering several charging states of the tank (values in kW).

Table 6: Top boundary.

Description	Material	k [W/m-K]	Length [m]
Layer 1	Carbon steel	47	0,1
Layer 2	Rockwool (insulation)	0,087	0,2

Table 7: Side boundary.

Description	Material	k [W/m-K]	Length [m]
Layer 1	Protective layer (refractory brick)	12	0,1
Layer 2	ISTRA CAC (concrete)	2,05	0,4
Layer 3	FCAC (thermal insulation)	0,07	0,6
Layer 4	Structural layer	1,63	0,8

Table 8: Bottom boundary.

Description	Material	k [W/m-K]	Length [m]
Layer 1	Protective layer (refractory brick)	12	0,1
Layer 2	ISTRA CAC (concrete)	2,05	0,7
Layer 3	FCAC (thermal insulation)	0,07	0,6
Layer 4	Structural layer	1,63	0,8
	Lightweight concrete	0,51	0,8
Layer 5[3]	Soil (TGQC-1)	6,23	15,1

[3] There is no convection below the tank because the reference temperature is for the ground. Therefore, soil was considered as the last layer.

Table 9: Heat losses through the walls ($T_{env} = 20\ ºC$).

Wall description	Charge				
	0%	25%	50%	75%	100%
Top boundary (Q_{top})	1,389	2,817	2,817	2,817	2,817
Side boundary ($Q_{side,t}$) @ ullage space	0,386	0,782	0,782	0,782	0,782
Side boundary ($Q_{side,b}$) @ MS	4,043	5,016	5,989	6,962	7,935
Bottom boundary ($Q_{bottom,o}$) @ periphery	0,216	0,216	0,216	0,216	0,423
Bottom boundary ($Q_{bottom,i}$) @ center	0,066	0,066	0,066	0,066	0,129
Total (Q_{losses})	6,099	8,898	9,871	10,844	12,087

As already described (Azevedo, 2017), the heat losses don't present a significant impact in the static thermal analysis of the tank. Although, the heat losses can twofold from a charge of 0% to 100%, the values are still very low when compared to the discharge power of the tank.

The tank discharge thermal power is identical to the solar field power output presented in Table 1 of 1800 kW. Considering that the maximum losses presented on Table 9 are near 12 kW, the losses with regard to discharge power are below 1% (0,67%).

Although the heat losses represent a small amount of power, their consequences in the TES tank performance should be assessed in WP5, in order to define the best operating strategy.

Although every charging states develops different temperature profiles inside the walls, the most challenging situation is presented by the full charge state (100%) when more losses are found. Table 10 and Figure 3 present the temperature profiles inside the walls for a tank fully charged (without thermocline). The layers considered for calculations are described in Figure 2 and equations (4), (9), (13), (18) and (22).

Table 10: Temperature inside the walls (tank fully charged and values in ºC).

Wall description	Layers				
	L_1	L_2	L_3	L_4	L_5
Top boundary	539,1	538,6	22,3	-	-
Side boundary @ ullage space	542,6	542,1	531,2	49,5	21,9
Side boundary @ MS	550,0	549,5	538,4	49,9	22,0
Bottom boundary @ periphery	550,0	549,6	534,3	149,0	126,9
Bottom boundary @ center	550,0	549,7	535,6	182,4	117,8

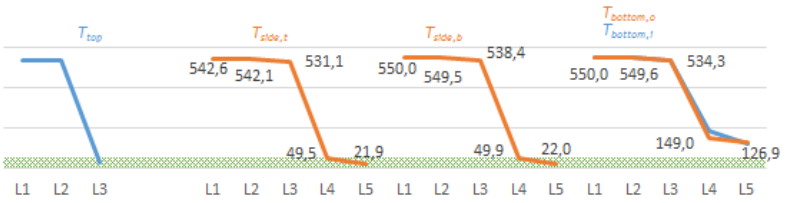

Figure 3: Temperature profiles inside the walls (charge = 100% and $T_{env} = 20\ ºC$).

The highlighted cells in Table 7 represent layers with a temperature limit of 50 ºC. Considering the 0,6 m of insulation (FCAC) in those walls, side boundary complies with the constraint up to an exterior temperature of 20 ºC and a wind speed of 6 m/s. However, when the calculation is made considering an environmental temperature of 35 ºC (in Figure 4 is possible to verify that from May to October the peak temperature is above 35 ºC), the temperature between the insulation layer and **the structural concrete layer reaches 63,7 and 64,1 ºC,** respectively.

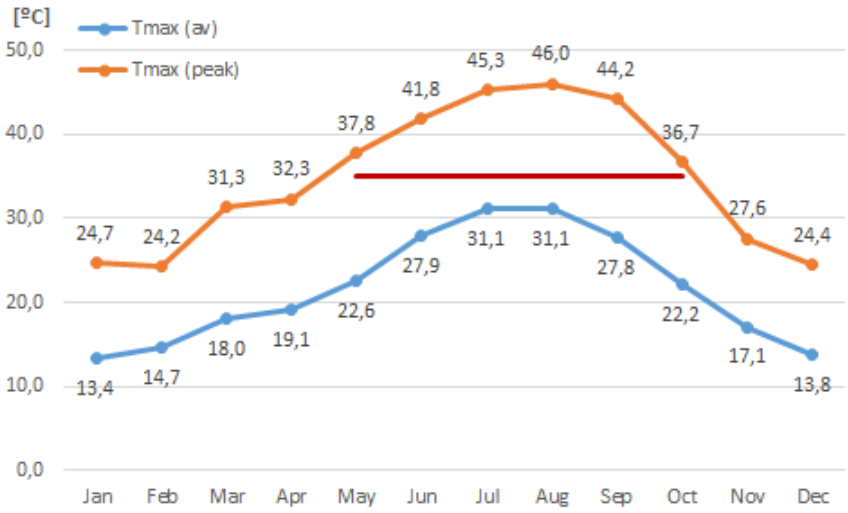

Figure 4: Maximum temperature in Évora (average and peak temperatures), IPMA (2017).

An additional problem seems to occur in the bottom boundary, with Layer 4 yielding the temperature of 149 ºC in the fully charged scenario. In the remaining scenarios (e.g. with some thermocline formed and the minimum temperature in contact with L_1), the temperature reaches 85,0 ºC. **Both values are way above the temperature limitation.**

Concluding remarks

From the calculations hereby presented some topics are still open to discussion and others present difficulties to be overcome. In this section those situations are presented and discussed.

LNEG approach considered the EMSP as a power plant, instead of a research facility. Hence, we aimed for a setup sized for power production, instead of a thermal energy storage tank sized for a different purpose.

Turbine

Regarding the Siemens SST-060 turbine, the data on the turbine is not publically available. The chosen design point of 131 bar(a) and 530 ºC, as well as the power output of 720 kW, are generic, considering that the only available data states a maximum pressure of 131 bar(a) and a maximum temperature of 530 ºC.

The SST-060 turbine power output ranges from roughly 500 kW to 6 MW. Other possible model from the same manufacturer, the SST-050, presents a maximum power output up to 750 kW that we considered to be below the intended available power.

The SST-060 turbine can either be used as a back-pressure turbine or a condensing turbine. In the present situation, the choice of a condensing turbine was considered to be more suitable although the maximum condensing pressure is not available. Considering that the SST-110 presents a condensing pressure up to 80 mbar(a), the condensing pressure of 125 mbar(a) was considered for the SST-060. Additionally, the isentropic efficiency of both the turbine and the pump are also unknown. For the present pre-design, both values were considered to be 85%.

The design point for the turbine sets the inlet enthalpy and the condenser working pressure which defines the outlet enthalpy after the turbine expansion. The difference of enthalpy between those two points are the main variables to compute the water/steam mass flow in a Rankine cycle, providing the turbine output power is known. Moreover, the water/steam mass flow and the enthalpy difference between the water at steam generator inlet and the steam at the outlet defines the input power for the power block and, consequentially, the capacity of the TES device for the desired autonomous working period of the power block. Therefore, the values considered here decreased the thermal capacity demand of the tank from 20,6 MWh to 16,9 MWh.

The values here considered pertain some impact in the dimensions of the tank, thus considering that no turbine will be installed at the location, **the values here presented can be revisited as the Consortium see fit**[4].

[4] Providing that the final values are frozen before the next project meeting.

Buffer height

The difference between $V_{HSM,0}$ in Table 3 and V_{HSM} in Table 4 is due to the buffer height of 30% considered to allow the use, in the power block, of the thermal energy stored in the tank for the complete discharge period (t) of 8h even with a thermocline with 30% of HSM in height and no isothermal low temperature zone.

The values here considered pertain a significant impact in the dimensions of the tank without a really payback, thus considering that no turbine will be installed at the location **the values here presented can be revisited as the Consortium see fit[4]**.

Temperature inside the walls

With regard to the temperature inside the walls, it has been difficult to comply with the constraints of the structural concrete of 50 ºC temperature, both on the side and on the bottom boundaries. This problem was split in two different situations, the peripheral walls and the foundation where, up until now, the FCAC layer considered was calculated for a thickness of 0,6 m.

The boundaries' behavior are different but they are both addressed below.

Side walls

As described in both in Table 10 and Figure 3, the side walls barely comply with the temperature constraint with an environment temperature of 20 ºC. If the environment temperature increase to 35 ºC, which is perfectly possible at location as described in Figure 4, **the temperature in the structural concrete increases to near 64 ºC.** In order to decrease this temperature value to 50 ºC, a 1,25 m thickness FCAC layer would be needed (considering a charge of 100%).

As we understand, the wall temperature calculations present significant sensitivity to the environment temperature. Therefore, the working conditions for the side walls are not adequately met. Consequently, **either the structural concrete limitations or the insulation layer thickness should be revisited by the Consortium**.

Foundation

The situation in the FCAC layer applied to the foundation of the tank is of more concern. In no circumstances, the aimed temperature of 50 ºC was ever reached between the FCAC and structural concrete layers. In this situation the environment temperature does not play any role. Instead, the data on the soil is far more important.

However, although the data on the soil proceeds from a near location of the future TES tank, we do not know how representative it is. The Fourier law of conductivity was considered to calculate the thermal conductivity of the soil. The temperature data and respective depths were retrieved from Figure A1b. Moreover, the heat flux density considered at the location was extrapolated (Figure A1a) to a value of 0,055 W/m^2. Thus, calculated thermal conductivity was 6,23 W/m-K and, **in this conditions the temperature in Layer 4 is 149,0 ºC (considering a charge of 100%).**

Some geology colleagues are under the opinion that the calculated thermal conductivity is twice as bigger than the generic value for that type of soil (near 3,4 W/m-K). If this value was considered, the temperature in the structural concrete would be above 200 ºC (again, considering a charge of 100%).

Naturally, the fully charged tank is the worst case scenario as the stored thermal energy is maximum and the temperature in the bottom of the tank is also maximum. If 75% of charge is considered, the molten salts temperature in the bottom of the tank is 290 ºC instead of the full charge 550 ºC. In this situation (charge=75% and conductivity=6,23 W/m-K), a temperature of 85 ºC is calculated.

In every solution, the temperature between the FCAC layer and the structural concrete layer is always above the 50 ºC. Consequently, **either the structural concrete limitations or the insulation layer thickness should be revisited by the Consortium**.

Solid/liquid layers

Considering that the HSM was considered to have an average temperature ($T_{MS,av}$), the number and filler fraction of the multiple solid/liquid layers foreseen in the DoA were not addressed in this document, although they are going to be applied in WP5.

As discussed at the proposal stage of the project, an integer number of solid/liquid layers in the HSM will be considered with approximately 1,0 m height. Those layers will allow 4 different working modes, including 0% (without filler) and 100% (full of filler) and the intermediate levels of 33% and 67% and the fraction of filler to consider in each layer will be the same in all layers.

Annex 1: Location

The Molten Salt Testing Platform (MSTP) of UÉvora is located in:

Longitude: -8.0060

Latitude: 38.5280

Nearest well: TGQC-1 (Correia and Ramalho, 1998)

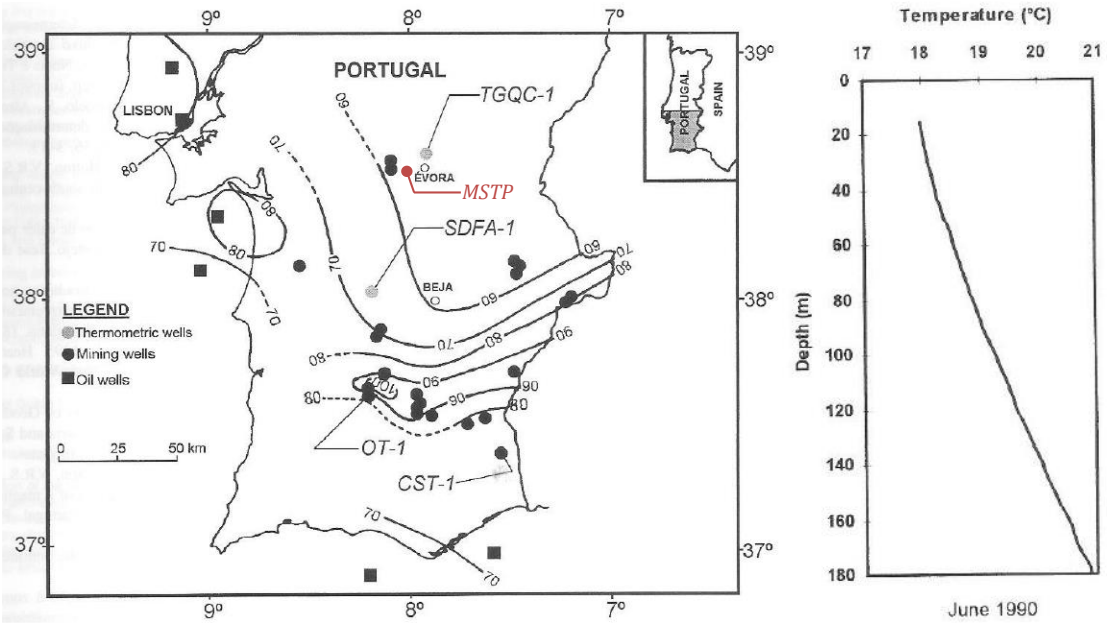

Figure A1: a) Location of MSTP and well TGQC-1 in the heat flux density map. b) Temperature log obtained in well TGQC-1.

References

Ryan Anderson, Liana Bates, Erick Johnson and Jeffrey F. Morris, 2015, "*Packed bed thermal energy storage: A simplified experimentally validated model*", Journal of Energy Storage, 4, pp 14 – 23.

P. Azevedo, 2017, "Thermal calculations for TES tank predesign", LNEG's internal report LEN-UER-2017-N01-IR, March.

E. Bayón and E. Rojas, 2014, "*Analytical description of thermocline tank performance in dynamic processes and stand-by periods*", Energy Procedia, 57, pp 617 – 626.

A. Correia and E. Ramalho, 1998, "*New heat flow density data from southern Portugal: a geothermal anomaly revisited*", Tectonophysics, 291, pp 55-62.

Scott M. Flueckiger, Zhen Yang, and Suresh V. Garimella, 2013, "*Review of Molten-Salt Thermocline Tank Modeling for Solar Thermal Energy Storage*", Heat Transfer Engineering, Vol. 34, Iss. 10,2013

IPMA, 2017, "Temperatura do ar, normais climatológicas – Évora, 1981-2010 (provisórias)", https://www.ipma.pt/pt/oclima/normais.clima/1981-2010/007/, visited in 09.05.2017.

Pei Wen Li, Cho Lik Chan, Jake Stephens, James. E. O'Brien, Jon Van Lew and Wafaa Karaki, 2011, "*Transient Heat Transfer and Energy Transport in Packed Bed Thermal Storage Systems*", INTECH Open Access Publisher, ISBN 9533075694, DOI: 10.5772/20979.

Libby C. *et al*, 2010, "Solar Thermal Storage Systems: Preliminary Design Study", EPRI (Electric Power Research Institute) Final Rept. 1019581.

R. Serrano-López, J. Fradera, S. Cuesta-López, 2013, "*Molten salts database for energy applications*", Chemical Engineering and Processing, 73, pp 87 – 102.